Review of bubble detector response characteristics and results from space

Article *in* Radiation Protection Dosimetry · September 2011

DOI: 10.1093/rpd/ncr358 · Source: PubMed

CITATIONS
14

READS
464

11 authors, including:

B. J. Lewis
Royal Military College of Canada
148 PUBLICATIONS **1,589** CITATIONS
SEE PROFILE

Harrt Ing
Bubble Technology Industries
109 PUBLICATIONS **1,124** CITATIONS
SEE PROFILE

Robert Andrews
Bubble Technology Industries
227 PUBLICATIONS **4,289** CITATIONS
SEE PROFILE

Rachid Machrafi
University of Ontario Institute of Technology
44 PUBLICATIONS **176** CITATIONS
SEE PROFILE

Radiation Protection Dosimetry (2011), pp. 1–21 doi:10.1093/rpd/ncr358

REVIEW OF BUBBLE DETECTOR RESPONSE CHARACTERISTICS AND RESULTS FROM SPACE

B. J. Lewis[1,*], M. B. Smith[2], H. Ing[2], H. R. Andrews[2], R. Machrafi[3], L. Tomi[4], T. J. Matthews[4], L. Veloce[4], V. Shurshakov[5], I. Tchernykh[5] and N. Khoshooniy[5]
[1]Royal Military College of Canada, Kingston, ON, Canada
[2]Bubble Technology Industries, Chalk River, ON, Canada
[3]University of Ontario Institute of Technology, Oshawa, ON, Canada
[4]Canadian Space Agency, St-Hubert, QC, Canada
[5]Institute of Biomedical Problems, Moscow, Russia

*Corresponding author: lewis-b@rmc.ca

Received January 25 2011, revised June 24 2011, accepted July 20 2011

A passive neutron-bubble dosemeter (BD), developed by Bubble Technology Industries, has been used for space applications. Both the bubble detector-personal neutron dosemeter and bubble detector spectrometer have been studied at ground-based facilities in order to characterise their response due to neutrons, heavy ion particles and protons. This technology was first used during the Canadian–Russian collaboration aboard the Russian satellite BION-9, and subsequently on other space missions, including later BION satellites, the space transportation system, Russian MIR space station and International Space Station. This paper provides an overview of the experiments that have been performed for both ground-based and space studies in an effort to characterise the response of these detectors to various particle types in low earth orbit and presents results from the various space investigations.

INTRODUCTION

Bubble detectors (BDs), which make use of superheated emulsions, are passive radiation detection devices that provide a tissue-equivalent neutron dose proportional to the number of bubbles formed in the detector[(1)]. Originally developed for nuclear industry applications, these detectors are based on earlier radiation detection devices which used dispersed, superheated liquid to detect ionising radiation but used the volume of evolved gas to measure the neutron dose[(2)]. The problem with the gas volumetric measurement (rather than bubble number) is that it implies that all superheated droplets must be the same size, which is difficult to achieve in the production process. There are currently two techniques for creating portable detectors containing dispersed superheated liquid. Both detectors operate under the same physics, but differ in the composition of their medium. The first, known as the superheated drop detector (registered trademark of Apfel Enterprises, Inc., New Haven, CT, USA), was developed by Apfel in the late 1970s and uses an aqueous gel as a detector medium[(3)]. In contrast, the bubble detector (registered trademark of Bubble Technology Industries Ltd., Chalk River, ON, Canada), developed by Ing, uses a polymerised gel instead, allowing bubbles formed through irradiation to be suspended within the detectors[(1)]. The polymer has an advantage in that it allows the bubbles formed to be recompressed for detector re-use. While the production of BDs has been attempted by several groups in different countries such as in Russia and India, the China Institute of Atomic Energy (CIAE) made similar detectors for both neutron detection and high-energy heavy ion track studies mainly for space applications[(4–6)]. However, despite utilising the ability to keep the bubbles in place with an elastic polymer medium, the CIAE detectors do not have the function to recompress the bubbles for additional use.

Early development of BDs, which are manufactured by Bubble Technology Industries (BTI), began with the BD-100R detector for health physics applications[(7)]. The BD personal neutron dosemeter (BD-PND), capable of detecting neutrons with energies varying from 100 keV to ~15 MeV, is currently the most common of the BTI detectors in commercial use (see Figure 1) and has been adapted for use in space[(8)].

BDs use microscopic superheated droplets maintained in a continuous meta-stable liquid state. These droplets are dispersed throughout a clear, elastic polymer and can detect neutrons through the formation of bubbles resulting from neutron interactions with the detector media[(7)]. Their lightweight, compact design, isotropic angular response and insensitivity to low-linear energy transfer (LET) radiation (such as electrons, X rays and gamma rays) make them ideal for personal neutron measurements. Unlike the BD-100R, BD-PNDs are able to compensate for temperature effects ranging from 20 to

37°C[9]. Once bubbles form, they are suspended in the elastic medium and can be counted visually or by a fully automated counter (e.g. BDR-III Automatic Bubble Reader) and then recompressed for detector re-use. The BD-PND is limited to ~300 bubbles, after which the overlapping of bubbles makes them difficult to count accurately. This limit can vary since bubbles continually grow in size slowly after irradiation and long periods of irradiation can lead to a distribution of bubble sizes.

BTI has also developed the BD spectrometer (BDS) for neutron energy spectra measurement. The BDS consists of six sets of detectors at six different energy thresholds: 10, 100, 600, 1000, 2500 and 10000 keV[9, 10]. Similar to the BD-PND, the BDS for space applications has been made to be reusable and is insensitive to low-LET radiation allowing its use in a mixed-radiation field. This spectrometer has been calibrated with monoenergetic neutron beams at particle accelerators and has been used in low earth orbit (LEO).

The BD technology has been well characterised for use in space[11–13]. This paper focuses on the characterisation of these detectors, including their response to particles other than neutrons, which is an important consideration for space application.

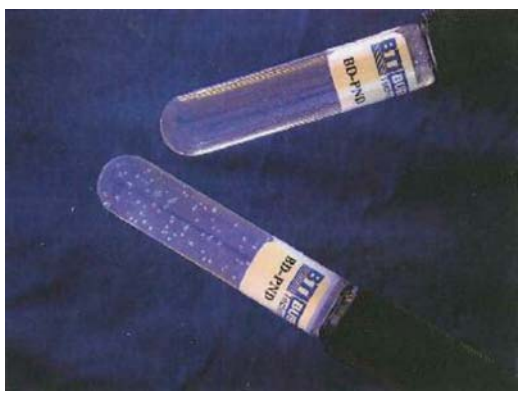

Figure 1. BD personal neutron dosemeter developed by BTI [Courtesy of BTI, taken from ref. (9)].

Physics of BDs

The formation of bubbles in the detector is based on the concept of induced nucleation through the use of superheated droplets. The first reasonable mechanism to describe this process was proposed by Seitz[14], and is known as the 'thermal spike' theory, where radiation produces localised temperature spikes within the superheated liquid, forming bubbles through the evaporation process.

In BDs, superheated droplets are kept in a liquid state at temperatures exceeding their boiling point, and are suspended in a clear plastic medium. Ionising radiation interactions deposit energy, causing localised sub-microscopic evaporation of the superheated fluid. Once these vapour cavities reach a critical radius (r_c), their expansion becomes irreversible and they grow until the whole droplet is evaporated[15]. The amount of energy and the critical size for bubble nucleation depends on the composition of the detector, as well as the amount by which the ambient temperature T of the fluid lies above the boiling point (i.e. the 'degree of superheat'). The critical radius (r_c) (m) is derived from the surface tension (γ) (N m^{-1}) of the liquid, the difference Δp (Pa) of the internal outward vapour pressure from the microscopic bubble (p_i) and the inward ambient pressure exerted by the elastic polymer (p_e)

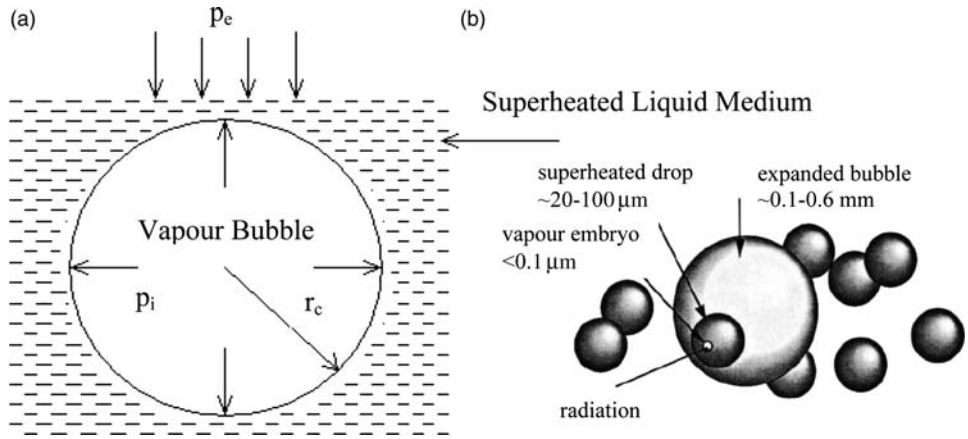

Figure 2. Schematic diagram showing (**a**) the pressures associated with a droplet surrounded by the elastic polymer of a BD[17] and (**b**) bubble formation from superheated droplets dispersed in a medium[43].

(see Figure 2)[16]:

$$r_c = \frac{2\gamma(T)}{\Delta p} = \frac{2\gamma(T)}{p_i - p_e} \quad (1)$$

If ionising radiation traversing the vicinity of a superheated droplet causes a nascent (or virtual) bubble to form that exceeds the local value of r_c, nucleation will occur and the bubble will continue to grow. However, if the critical radius is not reached, then the nascent bubble will compress under the surface tension and pressure of the medium.

The formation of a bubble of radius r_c requires a minimum amount of energy E_{min} (J). The amount of energy required to expand a bubble against the surface tension and ambient pressure is as follows[16]:

$$E_{min} = 16\pi\gamma^3(\Delta p)^2 + \left(1 + \tfrac{2}{3}\rho_v \frac{H}{M\Delta p}\right) \quad (2)$$

where ρ_v (kg m^{-3}) is the density of the vapour, H (J mol^{-1}) is the molar heat of vaporisation and M (kg mol^{-1}) is the molecular weight of the droplet material. Thus, E_{min} is the amount of energy required to form a bubble through vaporisation.

The predominant mechanism for the deposition of energy is due to the recoil ions from neutron interactions with the detector medium. Some interactions occur within the polymer, while some others occur within the superheated droplets. The recoil ions dissipate energy through the stopping power of the medium. Recoil ions that interact with the superheated droplets will produce a trail of microscopic bubbles where, if any of the bubbles exceeds r_c, they grow until the entire droplet is vaporised[17].

REVIEW OF GROUND-BASED TESTING

Neutrons

The early versions of neutron BDs were tested for their insensitivity to gamma radiation using a ^{60}Co source with a dose of up to 250 rads[1], and for their sensitivity to neutrons with a 200-μSv irradiation of Pu–Be neutrons. It was found that the rate of bubble formation could be controlled by altering the strength of the polymer medium or the quantity of the detector liquid, where there is a relationship between bubble formation and the amount of superheated liquid. The detectors were also affected by the ambient pressure, becoming completely insensitive to neutrons at pressurisation >70 psi. The detector response was also tested by varying the ambient temperature. Below a temperature of 24°C, there is insufficient superheat for bubble formation to occur. The temperature dependence can be offset by increasing the vapour pressure of the liquid.

Early experiments investigated the energy response of both the BD-100R and BDS devices over a wide neutron energy range[18]. Experiments at the National Institute of Science and Technology were carried out with neutron energies ranging from thermal to 144 keV, while the Van de Graff accelerator at the National Physical Laboratory exploited reactions of ^{7}Li(p,n), T(p,n), D(d,n) and T(d,n) to produce energies ranging from 0.033 to 0.627, 0.214

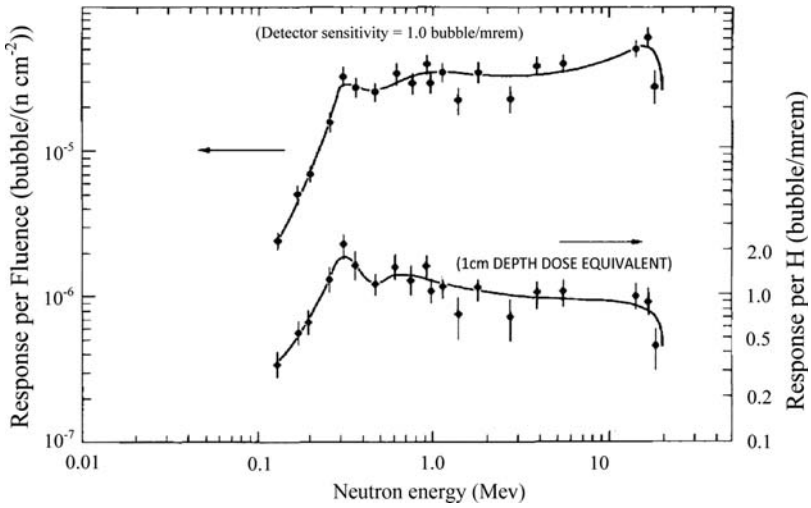

Figure 3. BD-PND normalised response per unit fluence (closed circles) and response per unit dose equivalent (closed diamonds). Conversion from fluence to dose equivalent based on NCRP Report No. 38[17].

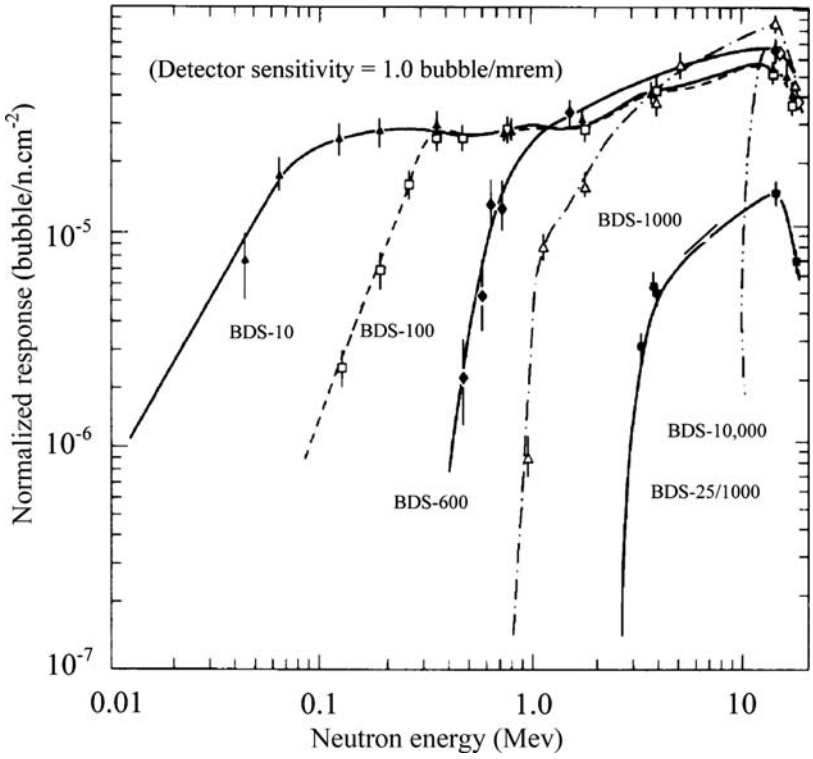

Figure 4. Normalised response per unit fluence for BDS at the six different thresholds[17].

to 2.22, 2.03 to 5.26 and 13 to 18 MeV, respectively. Further experiments were conducted with bare and moderated neutron sources of ^{252}Cf and Am–Be[18]. These early experiments were specifically used to determine the response of the BDS-10 and -100 detectors, and later the higher threshold detectors of BDS-600, BDS-1500 and BDS-2500.

In 1994, in order to quantify temperature-related effects on the response of BDs, Buckner *et al.*[19] carried out experiments at the Defence Research and Development of Canada – Ottawa facility using a 3-MeV KN Van de Graaf accelerator to produce monoenergetic neutrons. Studies were also conducted at this facility to determine the response-to-fluence of the BD-PND and BDS devices. These responses, normalised to 0.1 bubble μSv^{-1}, are shown in Figures 3 and 4[17]. The BD-PND, which has a 1-cm depth dose equivalent, shows a sharply increasing response from 100 up to ~200 keV, and then a relatively flat response to ~15 MeV. Studies with the BDS also confirmed that by altering the droplet formulation, different thresholds were achievable[17, 19]. A method for the fitting of the neutron response function is given in ref. (20). Additional ground-based accelerator studies were further carried out to better understand the high-energy response characteristics of the detector for space application [see text below and the section International Space Station (ISS) missions].

The BDS has been tested by Zanini *et al.*[10] in an experiment conducted at the Joint Research Centre in Italy, using a standard Am–Be source. Measurements were taken both with the bare spectrometer, and with the detectors contained within a tissue-equivalent anthropomorphic phantom. The resulting spectra were compared with calculated spectra using Monte Carlo simulations of the experimental set-up. Measurements were also carried out at the MAX-Lab photonuclear facility in Sweden, using photoneutrons generated from a bremsstrahlung photon beam. Results from these comparisons show good agreement between measurements and simulations.

The BD-PND and BDS detectors were also used in an integral, mixed-radiation field (i.e. consisting mainly of neutrons) at the European Organization for Nuclear Research/high-energy reference field (CERF) facility[21]. In this facility, a hadron beam collides with a copper target producing secondary particles filtered by an 80-cm thick concrete

shielding. This interaction gives rise to a neutron-component spectrum that closely resembles the radiation field created by cosmic rays at jet aircraft altitudes and in space. This field is well characterised using a number of devices (Bonner spheres and rem counters) as well as through simulation with the Monte Carlo code, FLUKA. It has an 'evaporation' peak at ~2 MeV and a 'spallation' peak at ~70 MeV, consistent with that observed at jet altitudes and space[21]. The possibility of extending the response of BDs to higher energy neutrons (>10 MeV) was experimentally investigated at the CERF facility by irradiating BDs enclosed in lead converters of various thicknesses[22]. Figure 5 shows comparison results measured with the BDS and a multisphere spectrometer after 6 h of irradiation[21].

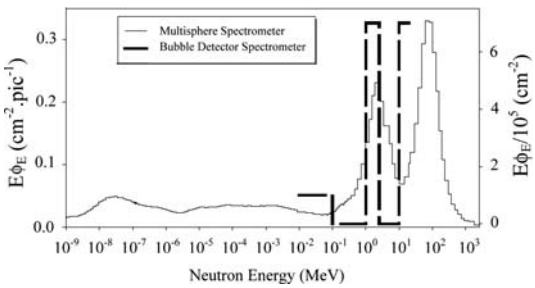

Figure 5. Comparison of neutron spectra measured at the ground-based facility at CERF using multisphere spectrometers (solid line) and BDS (dashed line)[21].

Additional testing of the neutron BD in mixed-radiation fields (i.e. neutron and photon field) was also carried out[23, 24]. BD-PNDs have further been used for personal neutron dosimetry[25], and evaluated in accordance with guidelines from the International Organization for Standardization for detector standardisation[26].

The BDs can be used to calculate an ambient dose equivalent $H^*(10)$ from the bubble counts. A response-to-dose equivalent calibration factor R_H can be specifically determined for a given neutron spectrum ranging in energy using dose conversion coefficients (see, for example, Figure 6)[21]:

$$R_H = \frac{M}{H} = \frac{\int_{E_{\text{lower}}}^{E_{\text{upper}}} R_\phi \phi_E \mathrm{d}E}{\int_{E_{\text{lower}}}^{E_{\text{upper}}} h_\phi \phi_E \mathrm{d}E} \qquad (3)$$

Here M is the number of bubbles observed, H is the measured (ambient) neutron dose equivalent, R_ϕ is the energy response function of the detectors, ϕ_E is the neutron differential flux and h_ϕ is the conversion factor [determined as $h_\phi = H^*(10)/\phi$ conversion coefficients (see the section ISS missions) where ϕ is

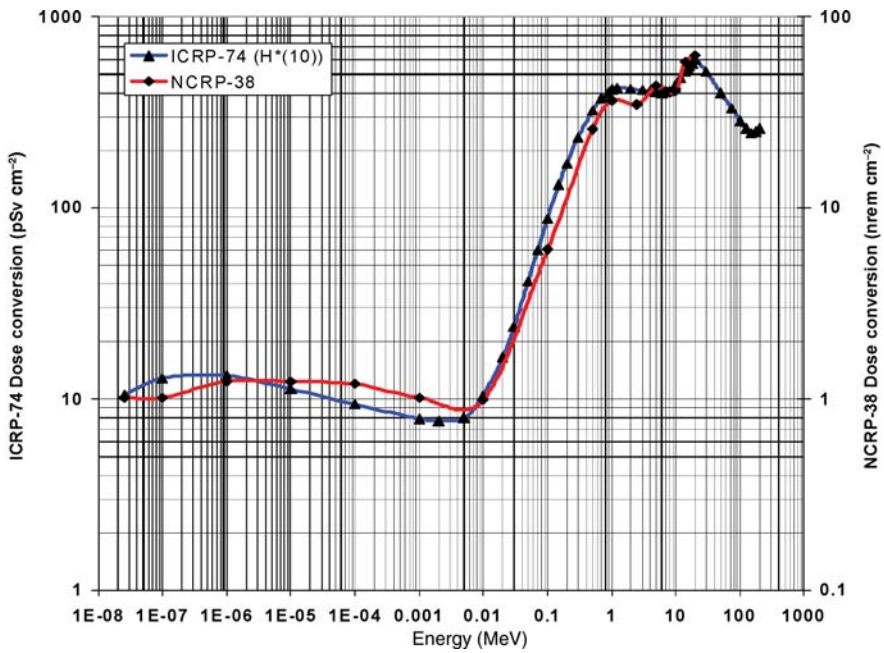

Figure 6. Dose conversion factors for neutrons.

the neutron fluence[13]]. A calibration factor for the BDs based on an Am–Be neutron spectrum is typically acceptable for terrestrial applications with NCRP-38 conversion coefficients. Equation (3) further indicates that for detectors with a nominal sensitivity of 6.0 bubbles μSv^{-1}, an R_H calibration factor of 3.7 bubbles μSv^{-1} is obtained for the neutron spectrum ϕ_E for the multisphere spectrometer shown in Figure 5 with an ICRP 60 recommendation. For the calculation in Eq. (3), E_{lower} $\sim 2\times10^{-8}$ MeV and E_{upper} $\sim$200 MeV. Hence, a correction factor of 1.62 from the manufacturer's standard calibration must be applied for the use of BDs for aircrew or space applications[27]. For instance, this calibration yields an agreement with Monte Carlo calculations of the CERF field as seen in Table 1[28]. Here the $E\phi_E$ versus E plot in Figure 5 can be converted to a differential flux plot and integrated to obtain an overall fluence rate. In this analysis, the dose equivalent is normalised to a precision ion chamber (PIC) count.

The temperature-compensated BD (i.e. BD-PND) includes a compensation material to adjust for sensitivity changes within the temperature range of 20–37°C. The reliability of this temperature compensation has been studied extensively [27, 29–31]. These studies show that the sensitivity of new detectors remains constant (within 20 %) over the stated temperature range; however, detectors of relatively high sensitivity will experience a gradual increase in sensitivity (~15 %) following repeated irradiations at room temperature over a 6-month period.

Protons

The effect of high-energy protons on the BD response has been studied in order to determine their contribution to the bubble count. Because high-energy protons are the dominant particle in LEO, peaking from 80 to 200 MeV and reaching energies of up to ~500 MeV (i.e. with a Greisen-Zatsepin-Kuz'min ultra-high energy cut-off for cosmic protons of $\sim10^{20}$ eV), this type of research is of interest for space applications of BDs. Cyclotron experiments conducted at Orsay investigated the proton response of BDs for energies from 200 MeV down to 0 MeV[8]. The detector response remained principally unchanged when the beam was blocked or when the detectors were placed outside the beam. This observation suggests little direct interaction by protons but rather a response to the neutron background produced by the proton beam striking different components of the accelerator. The upper limit for proton response in these experiments was estimated to be $<5\times10^{-5}$ bubbles per ($p{\cdot}cm^{-2}$) per (bubble μSv^{-1}).

Further experiments were carried out at the Proton Irradiation Facility located at the Tri University Meson Facility (TRIUMF) as part of the effort to characterise the BD response for space radiation[21]. The proton therapy facility is used for the treatment of ocular melanoma with 70 MeV proton beams, but has a beam energy range of 65–120 MeV. Measurements were performed using the 116 MeV beam line with a flux of 10^8 protons cm^2 s^{-1}. The proton beam entering into the experimental set-up was 81.7 MeV, with an energy of 5 MeV less entering into the detectors. At this energy, protons reach ~75 % of the total axial length of the detector. Individual detectors were arranged horizontally so that the beam particles could enter the bottom of the detector. This set-up also allowed a controllable variation of temperature from 10 to 70°C using a water bath and the ambient pressure between 0 and 60 psi using nitrogen gas to keep the detectors in a state of constant overpressure. The temperature was controlled for a constant superheat value of 0.35, which corresponds to an LET of 90 keV μm^{-1}. Bragg peaks were found up to 1000 keV with a peak thickness of ~2 mm. The thickness in the peak was due to straggling of the protons in the detector gel material, as confirmed by calculations with the stopping and range of ions in matter (SRIM) code[32]. The inability to observe a Bragg peak in higher threshold detectors (i.e. BDS-2500) was due to a temperature limitation with the melting point of the capping material (55°C).

A nuclear fragmentation separation experiment (NFSE) was also conducted at CERF to measure the charged particle response of the BDs where the detectors were surrounded by a plastic scintillator coincidence counter to separate the high-energy charged particles from the neutrons[27].

Detailed experiments were also performed using a proton beam at the cyclotron facility of the National Institute of Radiological Sciences in Chiba, Japan[12]. In this study, BDs with sensitivities of 0.31, 0.33 and 3.2 bubbles μSv^{-1} were exposed to protons with energies of 35, 50 and 70 MeV, respectively. The beams entered the detectors from the

Table 1. Integral measurements of the neutron field at CERF using BDs.

Detector type	Normalised equivalent dose $H_{NCRP\text{-}38,\ Am-Be}$ (pSv per PIC)[a]	Normalised dose equivalent $H^*(10)$ (pSv per PIC)	Monte Carlo calculated $H^*(10)$ reference values (pSv per PIC)
BDS set	210 ± 40	340 ± 70	254 ± 5
BD-PND	160 ± 30	260 ± 50	265 ± 5

[a]1 PIC=2.2×10^4 particles.

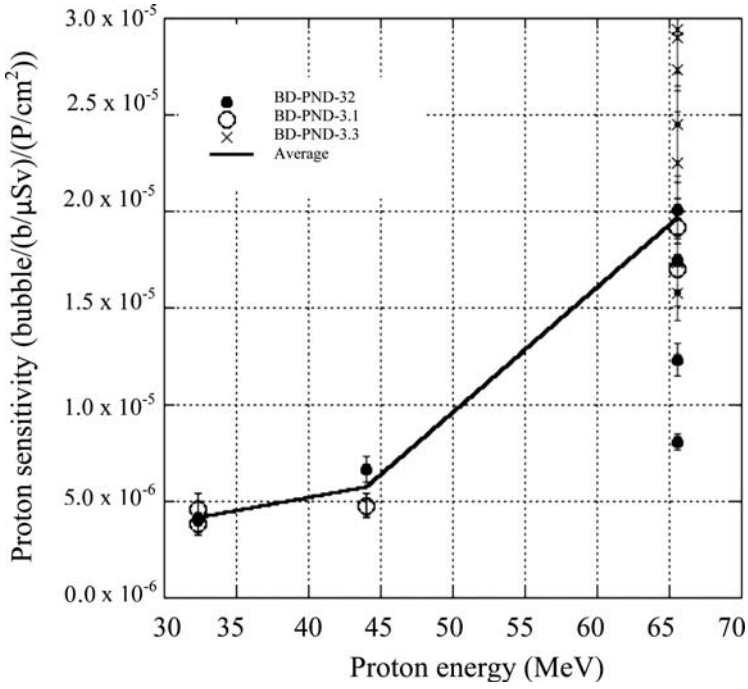

Figure 7. Measured proton sensitivities of the BD-PND; normalised according to the proton fluence, beam size and the detector neutron sensitivity[12].

bottom along their axis and their intensities were controlled at 10^4 protons s^{-1} using a 3-mm thick plastic scintillator placed upstream. To avoid producing secondary neutrons, the beam was narrowed to a diameter of 5 mm without a collimator. Detectors were irradiated until proton-track lengths could be visually measured within ± 1 mm. The mass stopping power for protons in the detector liquid was calculated to be 0.155 MeV $mg^{-1}{\cdot}cm^{-2}$ using SRIM. To confirm that bubbles were only formed from protons and not from neutrons, a detector was placed beside the main detector, where no bubbles formed. Additionally, bubbles were only observed on the near side of the detector, which would not have been the case if neutrons were present.

The proton sensitivity of the BD-PND was determined from the number of observed bubbles, which was divided by the number of incident protons, and normalised to the proton beam size (0.2 cm^2) and neutron detector sensitivity (see Figure 7). The detector sensitivities were corrected for temperature effects at 15.4°C by a factor of 0.8. These results are in good agreement with the upper limit of 5×10^{-5} bubbles per ($p{\cdot}cm^{-2}$) per (bubble μSv^{-1}) estimated in the Orsay experiment[8]. In comparison, proton sensitivities are 1 order of magnitude lower than that of neutrons. In particular, over a neutron energy range of 0.3–20 MeV for the BDS-100 (or BD-PND) detectors, the neutron sensitivities are in the range of $2–3\times10^{-4}$ bubbles per ($n{\cdot}cm^{-2}$) per (bubbles$\cdot\mu Sv^{-1}$).

The sensitivities in Figure 7 show a dependence on the proton energy. If the proton sensitivities are divided by the proton-track length in the detector (Figure 8), the normalised sensitivities become approximately independent of energy, with values of 5.0, 4.0 and 6.9×10^{-6} bubbles per ($p{\cdot}cm^{-2}$) per (bubble$\cdot\mu Sv^{-1}$) per cm for the 35, 50 and 70 MeV irradiations, respectively[33]. However, in a spacecraft, the detectors are irradiated in an isotropic fashion instead of in a head-on beam configuration. As follows from Cauchy's theorem for a body with a volume V and surface area S, the mean chord length through an arbitrary body is given as 4 V/S for isotropic irradiation[34]. Thus, the mean chord length for a cylindrical BD from Cauchy's theorem is the diameter of the detector (~1.7 cm) if all particles are able to completely traverse through the detector. Taking into account the shell thickness, and that the outer layer of the detector medium does not contain

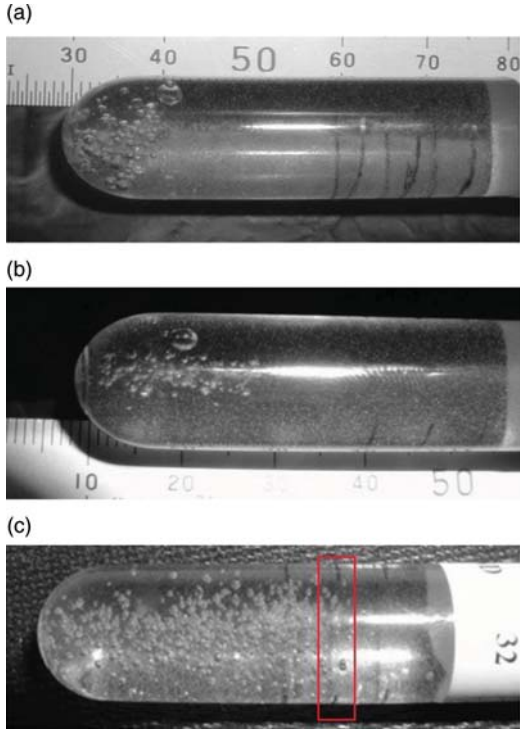

Figure 8. Bubbles formed with (**a**) 35-, (**b**) 50- and (**c**) 70-MeV protons. The scale length in millimeters is shown in the top two figures (**a**) and (**b**). Bubbles were observed from the bottom of the detector to the midline shown in the lower figure (**c**)[12].

superheated droplets, the effective track length is ~1.5 cm. This result is consistent with a more sophisticated code analysis using Geant 3.2.1, which similarly yields an average track length of 1.1 cm[33]. Hence, with an average sensitivity of 5.3×10^{-6} bubbles per (bubble μSv^{-1}) per p cm^{-2} per cm from the Chiba irradiations, and a given track length of 1.1 cm, the overall proton sensitivity is estimated as 5.7×10^{-6} bubbles per (bubble μSv^{-1}) per p cm^{-2} for space analysis (see the section Space experiments using BDs).

High atomic number - high energy particles

Experiments were performed at the heavy ion medical accelerator in the Chiba (HIMAC) Laboratory to characterise the response of BDs to high atomic number - high energy (HZE) particles[13]. Irradiations were performed on the BD-PND detectors using nitrogen (N) and argon (Ar) ions at 180 and 500 MeV u^{-1}, respectively. The HZE response depends on the amount of reduced superheat s and the given LET of the ion. The reduced superheat is a dimensionless quantity defined by[15]:

$$s = \frac{T - T_b}{T_c - T_b} \tag{4}$$

Here T is the temperature of the droplets during irradiation, T_b is the boiling (or saturation) point of the droplets and T_c is the critical temperature of the detector droplets. The length of the LET tracks defines the ion energy as well as the minimum LET for bubble formation.

Temperature-controlled experiments were performed at HIMAC to determine the amount of LET required to form bubbles[21]. A 180 MeV u^{-1} nitrogen ion beam and a 500 MeV u^{-1} argon ion beam were used. Individual detectors from the BDS were arranged in a set-up identical to the proton experiments performed at TRIUMF. For each type of detector, there was a specific pressure where bubble formation occurred. Through calculations, and from observations of where the bubbles began to form within the detectors, the threshold LET for bubble formation was determined for a given temperature. The dependence of LET versus the reduced superheat for HZE ions of Ar and N ions is shown in Figure 9, with the curve proposed by d'Errico for the minimum LET required for bubble formation[15]. The BD-PND response in the ion beams was measured to investigate the effects of temperature on detector response. At temperatures of 20, 31 and 38°C, the LET response of the detector was determined to be 231 ± 15, 231 ± 15 and 201 ± 40 keV μm^{-1}, respectively. Bubbles were also observed with an LET of 116 ± 40 keV μm^{-1} for the N ion at temperatures of 23 and 40°C. As the N ions require less LET to form a bubble compared with the Ar ion, this observation suggests that track structure plays an important role in the response of BDs. It is clear that temperature compensation for neutron detector response also maintains a threshold for HZE response. The superheat value of the BD-PNDs was found to be 0.3, consistent with the calculated value of 0.33.

SPACE EXPERIMENTS USING BDS

In LEO, neutrons are produced due to the interaction of protons and high-energy nuclei with the spacecraft (shielding) materials and albedo neutrons that leak from the underlying earth's atmosphere. The first experiments using BTI BDs in space to measure the neutron contribution occurred during a Canadian Space Agency (CSA) sponsored collaboration with Russia on board the BIOCOSMOS-9

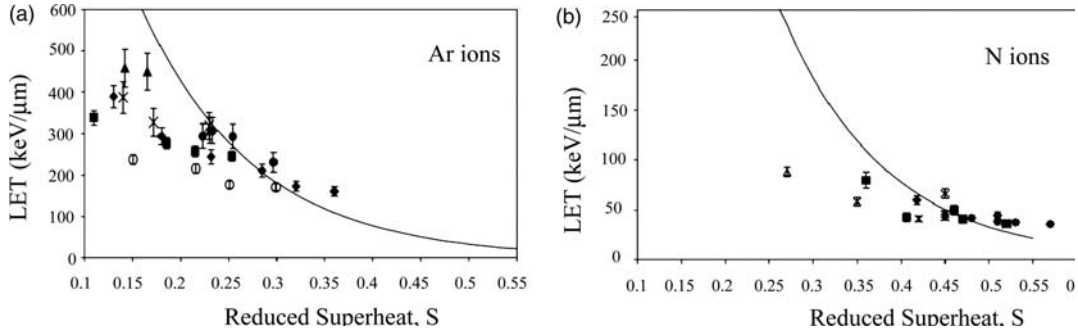

Figure 9. LET dependence on reduced superheat for Ar (left) and N (right) ions[15, 21].

(BION-9) satellite. Similar experiments were further performed on BION-10, -11, the Soviet/Russian Space Station MIR and the NASA Space Transportation System (STS) missions 81, 84, 86 and 89 (see the section BION, MIR and STS missions). Since then, these experiments were followed by the Matroshka-R set of experiments as a CSA–Russian collaboration on the ISS (see the section ISS missions).

BION, MIR and STS missions

With the goal of determining the neutron contribution to dose in space, BDs have been adapted for use in orbit. The first BION mission involved the use of BDs for neutron measurements on board the Biocosmos #9, where a BDS and six pairs of BDs (with thresholds from 10 to 1000 keV) were used to study the neutron spectrum in LEO and the neutron dose to cosmonauts[8]. The BDS was used over the 2-week mission and revealed a ~1 MeV neutron evaporation peak. A large number of higher energy neutrons (>10 MeV) were also observed, corresponding to 57 % of the total neutron dose. It was thought that these high-energy neutrons, with a fluence of 2×10^6 n·cm^{-2} and total equivalent dose of 0.75 mSv, resulted from proton bombardment of the satellite shell. The measurements from the detector pairs demonstrated that the neutron spectrum was similar throughout the satellite. When comparing the measurements between locations, it was found that the neutron equivalent dose was 0.37 mSv at a location with good shielding versus a dose of 0.82 mSv at another location. Subsequent BION missions, and later MIR and STS missions, also investigated the neutron dose and spectrum in LEO. The results of these missions, which spanned a time line of 7 years, are summarised in Table 2[16].

These missions measured a relatively constant neutron equivalent dose rate of 100 μSv d^{-1} throughout the 7-year period. Measurements performed on the STS missions gave comparable neutron dose rates to the earlier BION and MIR studies, but with a lower number of high-energy neutrons (only 25 % of the dose above due to neutrons >0 MeV). Figure 10 shows a comparison of the neutron spectra from the BION 9, 10 and MIR studies[16].

The neutron spectra in Figure 10 have similar features to that behind the concrete shielding at the CERF (see also Figure 5), as well as the spectrum measured in jet aircraft at 10.5 km, onboard the ISS as measured with Bonner ball detectors and the BDS (see the section ISS missions), and predicted for the STS-36, in Figure 11. All spectra typically show both evaporation and spallation peaks.

Thermoluminescence dosemeter (TLD) measurements made by Badhwar[35] from November 1992 to January 1993 during the MIR mission, i.e. at the same time as the BDS measurements in Figure 10 (lower panel), yielded an absorbed dose rate of 260 μGy d^{-1}. Assuming a typical tissue-equivalent proportional counter (TEPC) quality factor of 2.5 and a neutron fraction of 20 % of the charged particle dose equivalent, the TLD measurements imply a neutron dose equivalent rate of 260 μGy d$^{-1}\times2.5\times20$ %=130 μSv d^{-1}. This suggested value is in rough agreement with that measured in Figure 10 (lower panel) from the integrated spectrum (i.e. 92 μSv d^{-1}).

ISS missions

The BD-PND and BDS technology has been developed further as a space personal neutron detector (SPND) and a space BDS (SBDS) for space application on the ISS to measure the neutron field. 'Matroshka-R' phantom experiments were carried out in expeditions ISS-13, ISS-14, ISS-15 and ISS-16[36–38]. As discussed in the section Neutrons, the

Table 2. Summary of space missions using BDs from 1989 to 1998.

Date	Mission	Apogee (km)	Perigee (km)	Orbit inclination (degrees)	Neutron equivalent dose rate $H_{\mathrm{NCRP\text{-}38,Am-Be}}$ (μSv d^{-1})	Dose >10 MeV (%)
1989	BION-9	294	216	82.30	80	56
1993	BION-10	397	226	62.80	140	55
1993	MIR	419	399	51.64	92	51
1996	BION-11	401	225	62.80	80	47
Average					98	52
January 1997	STS-81	–	296	51.60	96	23
May 1997	STS-84	–	296	51.60	130	21
August 1997	STS-86	–	296	51.60	138	29
January 1998	STS-89	–	296	51.60	123	18
Average					122	23

manufacturer's uncertainty in the temperature compensation of the BD is ~10–20 %. The counting statistics for the device follows a Poisson distribution[39], so that the random error for the device is the square root of the number of bubbles observed, which gives rise to an uncertainty of ~10 % for a typical reading of ~100 bubbles). The error in the counting of the number of bubbles with the automatic reader is estimated at ~6 %. Hence, this uncertainty analysis therefore implies an overall upper-bound error of ~30–40 % for the ISS measurements.

During 2006–08, for the ISS-13, -14 and -15 expeditions, a total of nine experimental sessions were considered[38]. The majority of the measurements were made in the Zvezda service module and the Pirs docking module using BDs in the spherical phantom shown in Figure 12[37]. BDs were placed both inside and outside the phantom to simulate astronaut dose in the interior and exterior of the body. The detectors were irradiated for up to 5 days. During expedition ISS-16, more emphasis was placed on determining the neutron dose just inside the spherical phantom near the surface. The phantom was placed in the Pirs docking module, while various other detectors were placed in several other positions within the service module (e.g. starboard cabin, working desk and ceiling). For example, data combined from Sessions 8 and 9 are presented in Figure 13. As mentioned in the section Neutrons, a correction factor of 1.62 is applied to the manufacturer's standard calibration factor for the SPNDs in order to yield an ambient dose equivalent rate for the space neutron spectrum.

It is important to quantify the contributions of bubble counts derived from protons and heavy ions in the BDs in order to properly assess the neutron dose equivalent rates. For instance, the rate of bubble formation for a 4π-particle incidence for a given particle (p) is given as follows

$$\dot{N}_{\mathrm{b}} = 4\pi S_{\mathrm{d}} \int_{E_{\mathrm{lower}}}^{E_{\mathrm{upper}}} \phi_{\mathrm{p}}(E) S_{\mathrm{p}}(E)\mathrm{d}E \sim 4\pi S_{\mathrm{d}} \sum_{10\mathrm{MeV}}^{100\ \mathrm{GeV}} \phi(E) S_{\mathrm{p}}(E)\Delta E \quad (5)$$

where S_{d} (bubbles μSv^{-1}) is the detector sensitivity, $\phi_p(E)$ is the particle differential energy spectrum (particle cm^{-2} s^{-1} sr^{-1} MeV^{-1} nucleon^{-1}), S_{p} [bubble per (particle cm^{-2}) per (bubble μSv^{-1})] is the particle sensitivity and E_{lower} and E_{upper} are the integrand limits for the lower and upper values of particle energy, respectively. The number of bubbles N_{b} is therefore calculated for a given experiment duration, t (s), as:

$$N_{\mathrm{b}} = \dot{N}_{\mathrm{b}} t \quad (6)$$

The lower limit of energy of 10 MeV in the second relation in Eq. (5) corresponds to the value required for a proton to penetrate the shell of a BD.

A series of calculations were performed using the cosmic ray effects on micro-electronics (1996 Revision) (CREME96) code to determine the proton and heavy ion particle differential fluence rates $\phi_p(E)$ (Figure 14)[37, 40]. These functions can, in turn, be folded in with the ground-based response functions, S_{p}, (determined in the section Review of ground-based testing) for use in Eq. (5). Since the

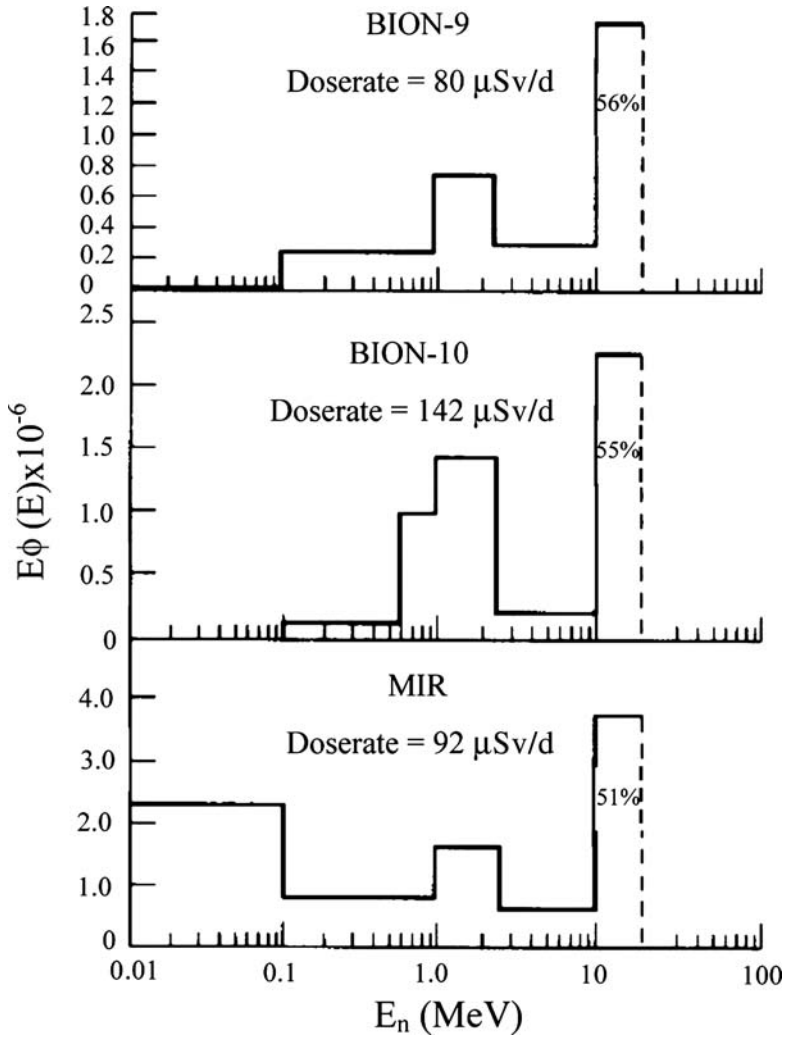

Figure 10. Neutron spectrum measurements from BION-9, -10 and MIR studies[16]. The neutron spectrum is integrated with respect to neutron energy to yield an estimate of the neutron equivalent dose rate ($H_{\mathrm{NCRP\text{-}83,\ AmBe}}$) (see also text in the section ISS missions).

proton sensitivity $S_p(E)$ for the BDs from the section Protons of 5.7×10^{-6} bubbles per (p·cm^{-2}) per (bubble μSv^{-1}) is independent of the proton energy, it can therefore be taken outside of the integral in Eq. (5) so that the integration needs to be performed only over the particle-energy spectrum. An isotropic (4π) incidence of protons can be further assumed for this calculation.

The energy spectrum of the ion depends on the thickness of the aluminium shielding of the spacecraft (see Figure 14). The CREME code (considering all ions $Z=1$–92) is able to match, with an assumed shielding thickness of ~8 g cm^{-2}, the Russian DB-8 dosemeter measurements in the service module during Sessions 7, 8 and 9 (ISS-15 and ISS-16) [i.e. observed absorbed dose rate of 150–350 μGy d^{-1} (mean of 240 μGy d^{-1})]. For this shielding thickness, the CREME code yields a proton fluence rate of 3.2×10^4 proton cm^{-2} d^{-1} sr^{-1}[37]. Hence, using Eq. (5), the contribution to the bubble count from protons for unit detector sensitivity is $4\pi\times3.2\times10^4$ proton cm^{-2}d^{-1}sr$^{-1}\times5.7\times10^{-6}$ bubbles per (p·cm^{-2}) per (bubble μSv^{-1}) per (86400 s d^{-1})$=2.7\times10^{-5}$ (bubble s^{-1}) per (bubble μSv^{-1}).

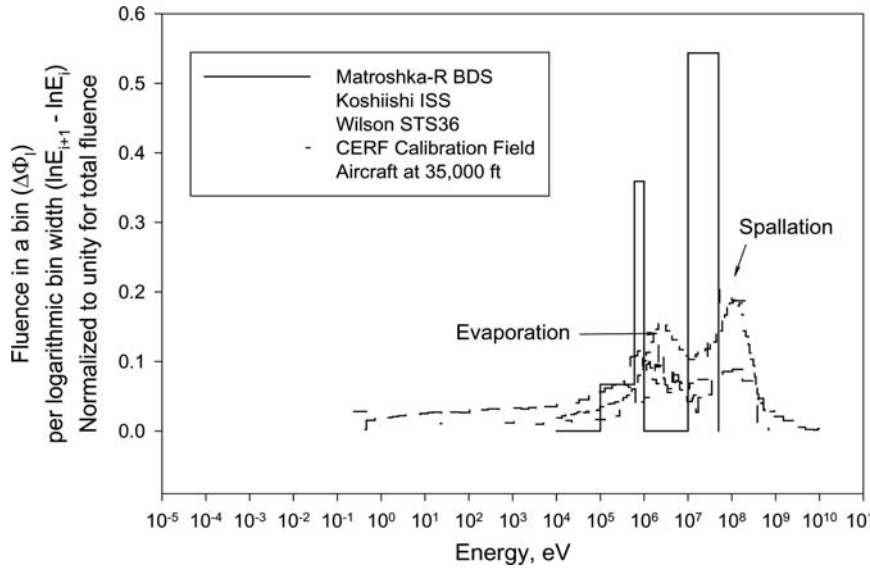

Figure 11. Comparison of the neutron spectrum at the CERF calibration facility, at jet aircraft altitudes and in space (adapted from ref. (44)).

Figure 12. Matroshka-R Phantom.

Given the detector sensitivity (S_d), measurement duration time (t=447000 s) and bubble count from Session 8 of ISS-16, the predicted number of bubbles can be compared with the actual bubble counts in Table 3. Thus, this analysis shows that the maximum contribution from protons to the total bubble count in the BD is ~2 %.

Similarly, charged particles heavier than protons can also contribute to the bubble count, with contributions from each ion from He (Z=2) to U (Z=92), governed by their cosmic abundances (see Figure 15). Elements heavier than Fe have such low abundances that they can be neglected. These ion contributions can also be estimated using calculated fluence rates with CREME96. The heavy charged particles can interact in a BD in two ways: (1) from their direct energy loss due to their LET, which provides sufficient energy loss for bubble nucleation or by (2) an elastic collision where their energy is transferred to a constituent recoil ion of fluorine[37]. Experiments performed at Chiba, as detailed in the section HZE particles, have demonstrated that bubble formation is dependent on LET, i.e. irradiations with N, Ar and Kr charged particles yield the LET threshold for bubble formation (which is different for each ion). As an overestimate for the heavy ion contribution, it is assumed that every particle above the LET threshold will form a bubble if it strikes a droplet. The probability of bubble formation can be given

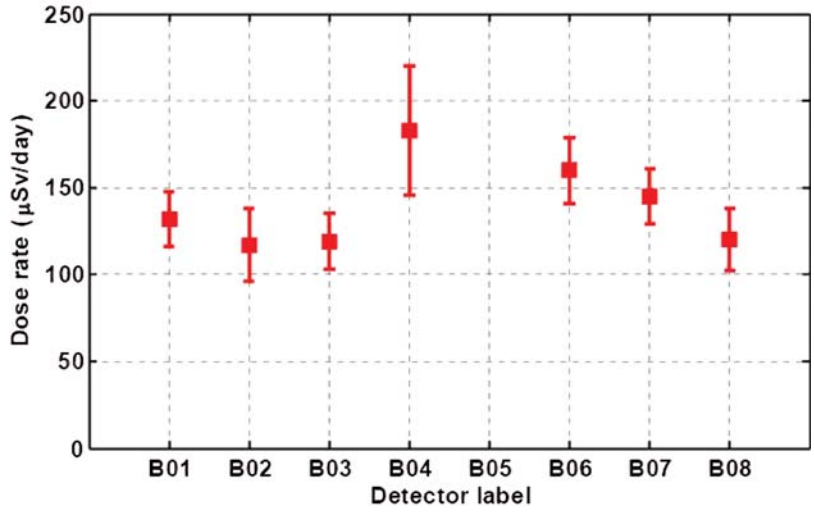

Figure 13. Summed data from Sessions 8 and 9 of the Matroshka-R Experiment.

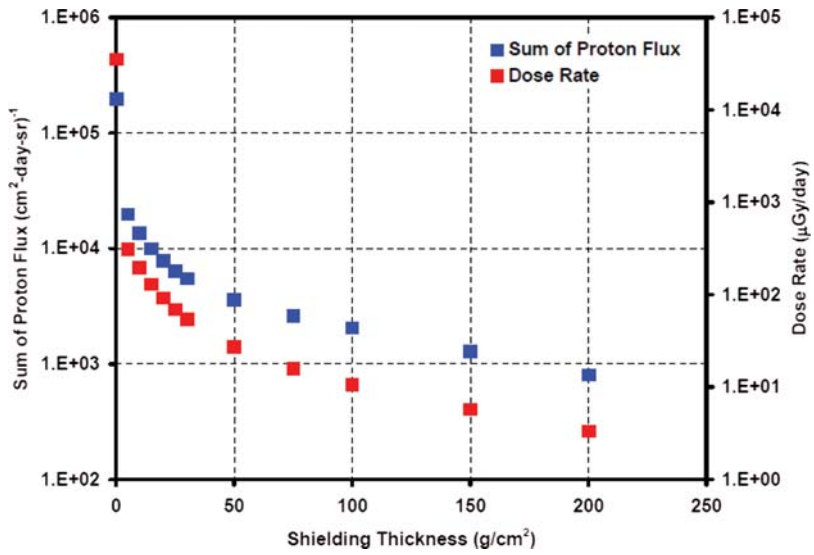

Figure 14. Proton fluence rate and total ion dose rate as a function of Al shielding based on CREME 96 code calculations.

by[37]:

$$P_{bf} = 1 - e^{(-n\sigma x)} \quad (7)$$

where n is the number of droplets per unit volume (= 10 000 droplets per cm^3), σ is the cross section (cm^2) of a droplet (i.e. diameter 20 μm) and x is the distance (cm) travelled (as calculated with the SRIM code) while its LET is above the threshold required to form a bubble. As discussed, critical LET values for ^{14}N and ^{40}Ar were measured at Chiba, while values for other ions can be obtained with mass scaling (see Table 4). As seen in Table 4, the probability of forming a bubble is higher for the heavier (i.e. less abundant) ions but this is off set by their decreasing abundance.

The maximum number of bubbles formed by LET of heavy ions is the product of the bubble-formation probability and the number of particles striking the detector as obtained from CREME calculations, using a shield thickness of 8 g cm^{-2}. In this

Table 3. Results from Session 8 of the Matroshka-R experiment during Expedition ISS-16 in February 2008.

Detector label	B01	B02	B03	B04	B06	B07	B08	Mean
Sensitivity (bubbles mSv^{-1})	123	117	111	111	99	93	86	106
Bubbles due to protons	1.5	1.4	1.3	1.3	1.2	1.1	1.0	1.3
Observed bubbles	72	71	64	105	73	71	48	72
Proton contribution (%)	2.1	2.0	2.0	1.2	1.6	1.6	2.1	1.8

calculation, only ions in a certain energy range are considered, defined by the minimum energy required to enter the detector and the maximum energy for which ions can deliver the critical LET value (Table 4). Thus, again assuming a 4π-incidence of ions, the bubble contribution due to heavy ions is shown in Table 4. These values can be compared with bubble count data taken for detector B01 from Session 7 of ISS-15. Thus, the contribution from the sum of these four ions is less than ~0.11 % due to any direct energy loss from the ions themselves.

The heavy ions can also lead to bubble formation due to knock-on recoil ions of the constituent materials. The measured sensitivity for protons can be scaled for each heavy-ion species assuming that a p+^{19}F reaction is responsible for bubble creation by protons and that the X+^{19}F reaction is responsible for bubble creation by a heavy-ion X. The cross section (σ) for interaction of two nuclei is given by[37]

$$\sigma_{pt} = \pi r_0^2 \left(A_p^{1/3} + A_t^{1/3} - b \right)^2 \quad (8)$$

where σ_{pt} is the cross section for the interaction of projectile (p) and target (t) nuclei; A_p and A_t are the mass numbers of the projectile and target nuclei, respectively; the radius r_0=1.23 fm; and b is an overlap parameter:

$$b = 1.56 - 0.2 \left(A_p^{1/3} + A_t^{1/3} \right)^2 \quad (9)$$

It is assumed that this parameterisation is also valid for proton interactions with the ^{19}F target. Using Eqs (8) and (9), the cross section for a particular ion species with the ^{19}F target can be estimated. By scaling to the p+^{19}F cross section and using the sensitivity of the BD to protons, the sensitivity of the detector to each heavy ion can be determined. The number of bubbles due to nuclear interactions of heavy ions can be calculated using the detector sensitivity and the predicted CREME96 fluence rates for a 4π incidence. The results of the calculation are shown in Table 5, using data for detector B01 from Session 7 of ISS-15 for comparison. The sum of the nuclear-interaction contribution of these four ion species is 0.18 %.

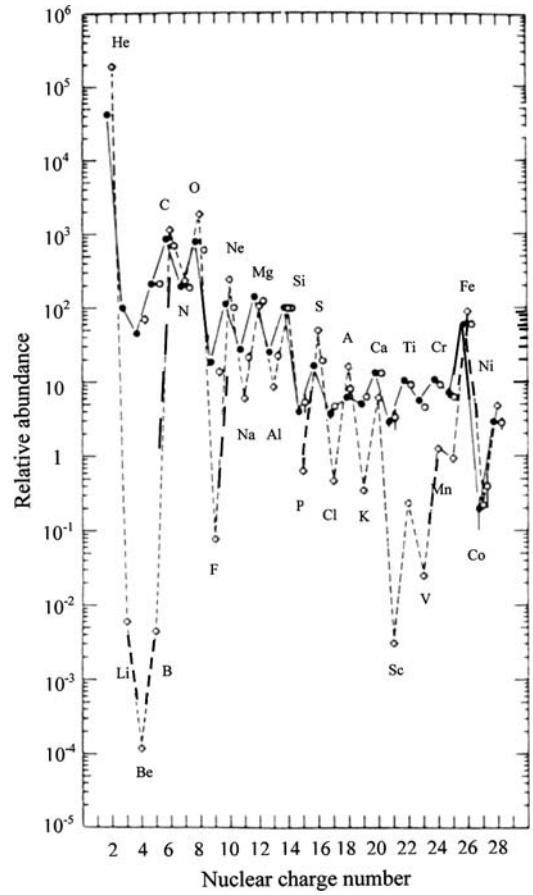

Figure 15. Abundances of elements relative to silicon (=100) in galactic cosmic radiation: (closed circles) low-energy data, 70–280 MeV nucleon^{-1}; (open circles) high-energy data, 1000–2000 MeV nucleon^{-1} compared with the solar abundances (open diamonds). Taken from ref. (45).

Hence, all charged particles (i.e. protons and heavy ions) are estimated to contribute less than ~3 % to the observed bubble count. Thus, the BD dose rates mainly reflect a neutron contribution. The neutron BD count rates can be further compared with those estimated with Eq. (5), given the BD

Table 4. HZE particle contribution to the bubble count due to LET during the Matroshka-R experiment.

Ion species	Minimum energy (MeV)	Maximum energy (MeV)	Threshold LET (keV μm^{-1})	Time (Min)	x (cm)	Observed bubbles	Probability	Bubbles due to LET (%)
^{4}He	35	150	100	10 144	0.0035	99	1.88×10^{-5}	0.020
^{14}N	250	1000	150	10 144	0.121	99	6.50×10^{-4}	0.015
^{16}O	300	1300	150	10 144	0.181	99	9.72×10^{-4}	0.061
^{40}Ar	1100	5000	300	10 144	0.859	99	4.60×10^{-3}	0.010

Table 5. Nuclear-interaction contribution to the bubble count of HZE particles.

Ion species	BD sensitivity (bubble (ion $cm^{-2})^{-1}$ per μSv)	Time (min)	Observed bubbles	Bubbles due to nuclear interaction (%)
^{4}He	3.47×10^{-5}	10 144	99	0.17
^{14}N	6.54×10^{-5}	10 144	99	0.0020
^{16}O	7.05×10^{-5}	10 144	99	0.0051
^{40}Ar	1.24×10^{-4}	10 144	99	0.00020

response to neutrons and a measured neutron differential flux:

$$\dot{N}_b \sim 4\pi S_d \sum_{0.25MeV}^{100\ MeV} \phi_n(E) S_n(E) \Delta E \qquad (10)$$

For example, the differential flux for neutrons $\phi_n(E)$ has been measured in the study of Koshiishi *et al.* in 2007 on board the ISS using Bonner Ball Neutron Detectors (BBND) as shown in Figure 16[41]. The BD response function for the various detectors used in the space SBDS, S_n, is shown in Figure 17 (for a detector sensitivity of 0.1 bubble μSv^{-1}). For the ISS ambient dose equivalent rate measurements, the most recent response function for the BDS-100 in Figure 17 can be used for the SPND. This response has been specifically extended to include additional high-energy neutron response measurements at 100 and 200 MeV as performed in recent ground-based accelerator studies at the iThemba laboratory for a quasi-monoenergetic beam. Thus, Eq. (10) with the data in Figures 16 and 17 yield the results shown in Table 6 for Session 8 of the Matroshka-R experiment. There is reasonable agreement (i.e. factor of 2) between the number of bubbles predicted using the proposed neutron differential spectra of Koshiishi *et al.* and that observed in the Matroshka-R experiment. An under prediction may result in part from the fact that the neutron spectrum in Figure 16 does not include higher energy neutrons >100 MeV, as well as due to different shielding effects.

The response data in Figure 17 were further used to develop a response matrix (up to 50 MeV), and an extended response matrix (up to 300 MeV using the iThemba data), for spectral analysis with the SBDS as given in the Appendix.

Table 7 also shows dose equivalent rates obtained with the SPNDs (A09 and A10) for additional Matroshka sessions in ISS-20 and ISS-21. Dose equivalent rates obtained with the BDs is also compared with measured absorbed dose rates and dose equivalent rates obtained with the US TEPC and the Russian DB-8 dosemeters [33, 37]. All devices were co-located in the service module for this session. As seen in Table 7, the TEPC absorbed dose rate lies within the spread of the DB-8 results. The SPND dose equivalent rate is lower because it is only due to neutrons, suggesting a neutron fraction of ~27 % of the total dose equivalent.

During these Sessions in the period of 13–18 August 2009, spectral measurements were performed with the SBDS in the Service Module P327. The SBDS spectral results shown in Figure 18(a) and (b) were derived with an unfolding based on the response matrices from 0 to 50 MeV and 0 to 300 MeV in the Appendix. The dotted lines represent the maximum and minimum fluence calculated by varying the bubble count in each detector by 1 standard deviation. The unfolded spectrum is presented as an $E\phi$ (E) plot, since this type of representation better reveals the given spectral features. The Matroshka spectrum, using the 0–50 MeV response matrix, is also shown in Figure 11 in comparison with other spectra from the CERF calibration, at jet aircraft altitudes and in space. All plots show a strong presence of an evaporation peak and a higher energy spallation peak. The SBDS spectral features are shifted in energy slightly as compared with the other spectra. Using the larger-range response matrix (0–300 MeV), however, places the spallation peak closer to that seen in the other spectra. This discrepancy can be explained by the fact that the BDS measurements have less resolution compared with the other methods since only six detectors are used for the spectral unfolding. Moreover, the unfolding procedure itself gives rise to poorer

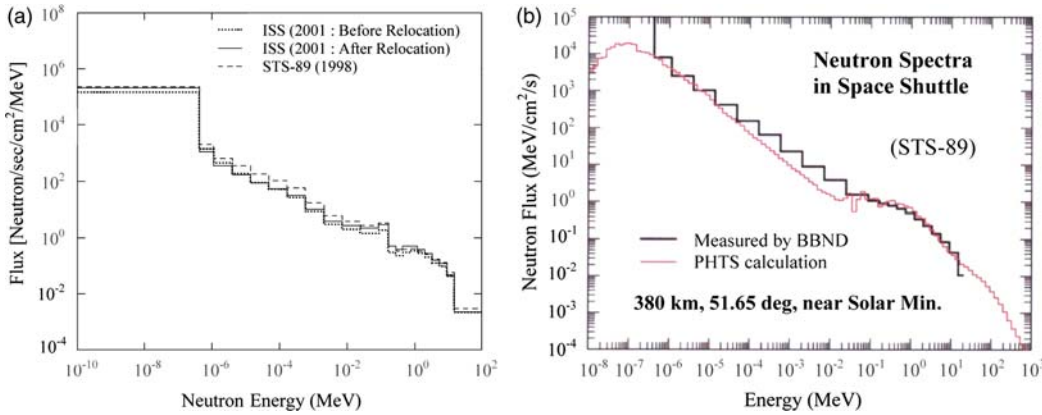

Figure 16. Orbit-averaged neutron spectra as measured with BBND on the space shuttle (STS-89) (380 km, 51.56° near solar minimum conditions) and ISS from (**a**) refs. (41) and (**b**) ref. (46). A comparison of the STS-89 measurement to a calculation with the PHITS particle and heavy-ion transport code is also shown[46].

statistics compared with the dose rate measurements with the SPNDs.

The dose rates can be further extracted from the unfolded spectra using fluence-to-ambient dose equivalent $H^*(10)$ conversion coefficients from ICRP 74 (see Figure 6). Two dose-rate values are given for each given matrix unfolding in the Appendix, using either the response matrix to 50 MeV or the extended one to 300 MeV. The percentage of the dose in the highest energy bin (i.e. dose >15 MeV) is also given in Table 8. The SBDS dose values are generally consistent with the SPND results, and with measurements performed using the other devices (although the uncertainty is greater because of the poorer statistics with the SBDS). The results are also similar to those obtained using the BDS in earlier space missions. The values of H_{50} and H_{300} are almost identical, which provides confidence in the extended response matrix and in the unfolding process. This analysis suggests that ~40 % of the neutron dose received in space is due to high-energy neutrons >15 MeV, which is consistent with findings of other researchers[42], indicating the importance of high-energy neutrons to the dose assessment.

CONCLUSION

(1) BD technology developed by BTI has been used for neutron radiation monitoring in space since 1989, including missions on Bion satellites, MIR, STS and the ISS. During 2006–09, BDs were used in the Matroshka-R study aboard the ISS during several expeditions (ISS-13, -14, -15, -16, -19, -20 and -21). From these experiments neutron dose measurements and neutron energy spectra were determined.

(2) Ground-based accelerator studies indicate that the BDs have a proton-response sensitivity of $\sim 5.7 \times 10^{-6}$ bubble / (bubble μSv^{-1}) per (p cm^{-2}). Studies at the HIMAC have demonstrated a relationship between the reduced superheat and LET of different heavy-ion species. Bubble formation can also occur from these heavier charged particles due to LET and direct nuclear interactions. Using response data for neutrons, protons and heavy ions, based on a comprehensive review of all the literature bubble-detector data derived from ground-based (accelerator) studies, along with differential flux data calculated using the CREME code, calculations were performed to determine the contribution of charged particles to bubble formation based on experiments conducted on the ISS (item 3).

(3) The neutron contribution can make up to ~30 % of the total dose equivalent due to the production of higher energy neutrons from interaction of mostly protons with the spacecraft shielding and albedo neutrons that leak from the underlying earth's atmosphere. A large fraction of the dose equivalent of neutrons (~40 %) is received from neutrons with energies >15 MeV. A recent study with the Matroshka-R phantom in space aboard the ISS indicates that the overall ion contribution to the bubble count is typically <3 %, and therefore bubble technology provides a crucial estimate of the neutron radiation field in space.

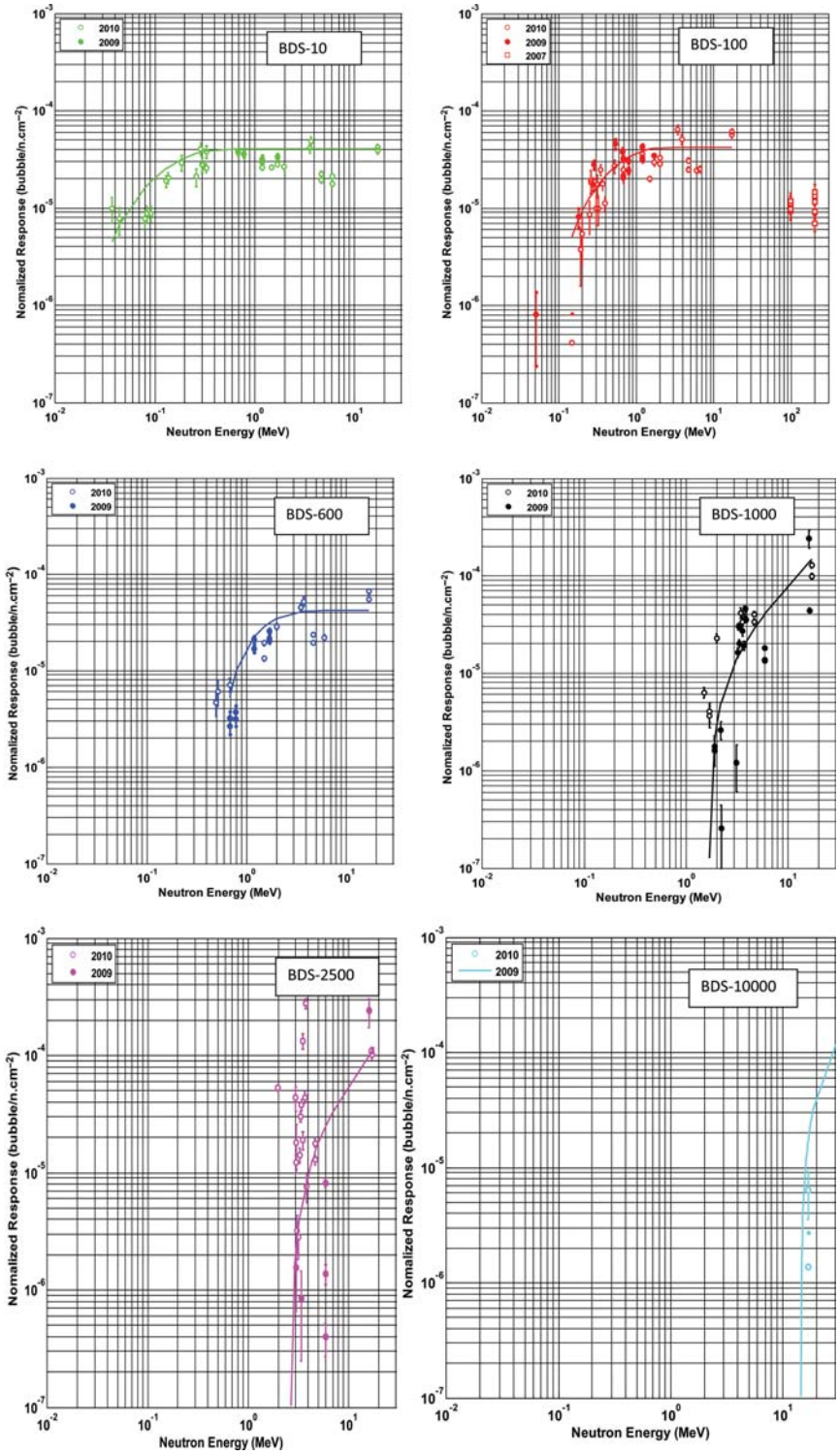

Figure 17. Response function for the SBDS (0.1 bubble μSv^{-1} detector sensitivity).

Table 6. Predicted and measured number of bubbles due to neutrons for Session 8 of the Matroshka-R experiment.

$4\pi\Sigma^{'}[\phi_n(E) * S_p(E)*\Delta E]$ (bubble/(bubble μSv^{-1}) per second)	Detector label	Detector sensitivity, S_d (bubble μSv^{-1})	No. of bubbles per second	Time elapsed (s)	Theoretical number of bubbles	Measured bubble count (Matroshka-R Session 8)	Predicted/ measured
7.57E−04	B01	0.123	9.31E−05	44 7000	42	72	1.73
7.57E−04	B02	0.117	8.86E−05	44 7000	40	71	1.79
7.57E−04	B03	0.111	8.41E−05	44 7000	38	64	1.70
7.57E−04	B04	0.111	8.41E−05	44 7000	38	105	2.79
7.57E−04	B06	0.099	7.50E−05	44 7000	34	73	2.18
7.57E−04	B07	0.093	7.04E−05	44 7000	31	71	2.26
7.57E−04	B08	0.086	6.51E−05	44 7000	29	48	1.65
				Mean	36	72	2.01

Table 7. Comparison of SPND, TEPC and DB-8 results for Matroshka experiment measurements.

Detector	A09	A10	TEPC	DB-8 #1		DB-8 #2		DB-8 #3		DB-8 #4	
				U[a]	S[a]	U	S	U	S	U	S
Absorbed dose rate ($\mu Gy\ d^{-1}$)			277	378	372	278	307	302	295	225	257
Dose equivalent rate ($\mu Sv\ d^{-1}$)	200 ± 33[a]	166 ± 29[a]	675[b]								

U, unshielded; S, shielded.
[a]In units of $H^*(10)$.
[b]In units of H_{TEPC}.

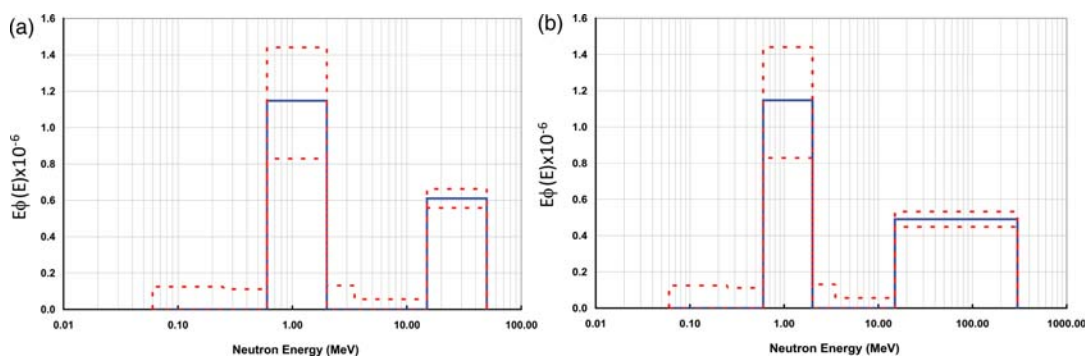

Figure 18. Neutron spectrum measured during ISS-20 and 21 with the SBDS using the (**a**) 0–50-MeV response matrix and the (**b**) 0–300-MeV response matrix.

Table 8. Spectroscopic SBDS ambient dose equivalent rates during ISS-20 and 21.

Session	Matroshka
H_{50} (μSv d^{-1})	$141 \pm 56\%$
Fraction of H_{50} >15 MeV (%)	45
H_{300} (μSv d^{-1})	$140 \pm 56\%$
Fraction of H_{300} >15 MeV (%)	44

ACKNOWLEDGEMENTS

The authors would also like to acknowledge the previous work of Drs. A.R. Green and L.G.I. Bennett of RMC in the ground-based testing of bubble technology.

FUNDING

The authors would like to acknowledge funding from the Canadian Space Agency for this study.

REFERENCES

1. Ing, H. and Birnboim, H. C. *A bubble damage polymer detector for neutrons*. Nucl. Tracks Radiat. Meas. **8**, 285–288 (1984).
2. Apfel, E. and Roy, S. C. *Instrument to detect vapour nucleation of superheated drops*. Rev. Sci. Instrum. **54**(10), 1397–1400 (1983).
3. Apfel, R. E. *The superheated drop detector*. Nucl. Instrum. Methods Phys. Res. A **162**, 603–608 (1979).
4. Guo, S. L. *Bubble detector investigations in china*. Radiat. Prot. Dosim. **120**(1–4), 491–494 (2006).
5. Guo, S. L., Li, L., Chen, B. L., Doke, T., Kikuchi, J., Terasawa, K., Komiyama, M., Hara, K. and Fuse, T. *Proton tracks in bubble detector*. Nucl. Instrum. Methods Phys. Res. B **198**, 135–141 (2002).
6. Guo, S.-L., Li, L., Chen, B.-L., Doke, T., Kikuchi, J., Terasawa, K., Komiyama, M., Hara, K., Fuse, T. and Murakami, T. *Status* of bubble detectors for high-energy heavy ions. Radiat. Meas. **36**, 183–187 (2003).
7. Cousins, T., Tremblay, K. and Ing, H. *The application of the bubble detector to the measurement of intense neutron fluences and energy spectra*. IEEE Trans. Nucl. Sci. **37**(6), 1769–1775 (1990).
8. Ing, H. and Mortimer, A. *Space radiation dosimetry using bubble detectors*. Adv. Space Res. **14**(10), 73–76 (1994).
9. Bubble Technology Industries Inc. (2009). *Bubble detectors: neutron dosimeters*. http://www.bubbletech.ca/pdfs/BTI_BUBBLE_General_May72009.pdf.
10. Zanini, A., Fasolo, F., Visca, L., Durisi, E., Perosino, M., Annand, J. R. M. and Burn, K. W. *Test of a bubble passive spectrometer for neutron dosimetry*. Phys. Med. Biol. **50**, 4287–4297 (2005).
11. Hoffman, J. M., Harvey, W. F. and Foltyn, E. M. *Bubble dosimetry experience at Los Alamos National Laboratory*. Report for Los Alamos National Lab. Dosimetry: Users, Results and Trends. San Antonio (1995).
12. Takada, M., Kitamura, H., Koi, T., Nakamura, T. and Fujitaka, K. *Measured proton sensitivities of bubble detectors*. Radiat. Prot. Dosim. **111**(2), 181–189 (2004).
13. Andrews, H. R., Noulty, R. A., Ing, H., d'Errico, F., Lewis, B. J., Bennett, L. G. I. and Green, A. R. *LET dependence of bubble detector response to heavy ions*. Radiat. Prot. Dosim. **120**(1–4), 480–484 (2006).
14. Seitz, E. *On the theory of the bubble chamber*. Phys. Fluids **1**, 2–13 (1958).
15. d'Errico, F. *Fundamental properties of superheated drop (bubble) detectors*. Radiat. Prot. Dosim. **84**(1–4), 55–62 (1999).
16. Ing, H. *Neutron measurements using bubble detectors—terrestrial and space*. Radiat. Meas. **33**, 275–286 (2001).
17. Ing, H., Noulty, R. A. and McLean, T. D. *Bubble detectors—a maturing technology*. Radiat. Meas. **27**(1), 1–11 (1997).
18. Schwartz, R. B. and Hunt, J. B. *Measurement of the energy response of superheated drop neutron detectors*. Radiat. Prot. Dosim. **34**(1–4), 377–380 (1990).
19. Buckner, M. A., Noulty, R. A. and Cousins, T. *The effect of temperature on the neutron energy thresholds of bubble techology industries'* bubble detector spectrometer. Radiat. Prot. Dosim., **55**(1), 23–30 (1994).
20. Lessard, L., Hamel, L.-A. and Zacek, V. *Neutron response functions for superheated droplet detectors*. IEEE Trans. **46**(6), 1907–1912 (1999).
21. Green, A. R., Andrews, H. R., Bennett, L. G., Clifford, E. T., Ing, H., Jonkmans, G., Lewis, B. J., Noulty, R. A. and Ough, E. A. *Bubble detector characterization for space radiation*. Acta Astronautica **56**, 949–960 (2005).
22. Agosteo, S., Silari, M. and Ulrici, L. *Improved response of bubble detectors to high energy neutrons*. Radiat. Prot. Dosim. **88**(2), 149–155 (2000).
23. Bassler, N., Knudsen, H., Møller, S. P., Petersen, J. B., Rahbek, D. and Uggerhøj, U. I. *Bubble detector measurements of a mixed radiation field from antiproton annihilation*. Nucl. Instrum. Methods Phys. Res. B **251**, 269–273 (2006).
24. Vanhavere, F., Coeck, M. and Lievens, B. *The response of the BTI bubble detectors in mixed gamma-neutron workplace fields*. Radiat. Prot. Dosim. **125**(1–4), 309–313 (2007).
25. Vanhavere, F., Vermeesch, F., Chartier, J. L., Itie, C., Rosenstock, W., Köble, T. and d'Errico, F. A. *Comparison of different neutron spectroscopy systems at the reactor facility VENUS*. Nucl. Instrum. Methods Phys. Res. A **476**, 395–399 (2002).
26. Vanhavere, F. and d'Errico, F. *Standardisation of superheated drop and bubble detectors*. Radiat. Prot. Dosim. **101**(1–4), 283–287 (2002).
27. Green, A. R., Bennett, L. G., Lewis, B. J., Tume, P., Andrews, H. R., Noulty, R. A. and Ing, H. *Characterisation of bubble detectors for aircrew and space radiation exposure*. Radiat. Prot. Dosim. **120**(1–4), 485–490 (2006).
28. Mayer, S., Golnik, N., Kyllonen, J. E., Menzel, H. G. and Otto, T. *Dose equivalent measurement in a strongly pulsed high-energy radiation field*. Radiat. Prot. Dosim. **110**(1–4), 759–762 (2004).

29. Tume, P., Lewis, B. J., Bennett, L. G. I. and Cousins, T. *Characterization of neutron sensitive bubble detectors for application in the measurement of jet aircrew exposure to natural background radiation*. Nucl. Instrum. Methods Phys. Res. A **406**, 153–168 (1998).
30. Vanhavere, F., Thierens, H. and Loos, M. *Testing of the temperature compensated BD-PND bubble detector*. Radiat. Prot. Dosim. **65**(1–4), 425–428 (1996).
31. Vanhavere, F., Loos, M. and Thierens, H. *The life span of the BD-PND bubble detector*. Radiat. Prot. Dosim. **85**(1–4), 27–30 (1999).
32. Ziegler, J. F., Ziegler, M. D. and Biersack, J. P. *SRIM: the stopping and range of ions in matter*. www.SRIM.org (2008).
33. Smith, M. B. *et al.*. *Measurements of the neutron dose and energy spectrum on the International Space Station during expeditions ISS-16 to ISS-21*. Radiat. Prot. Dosim [submitted for publication].
34. Bell, G. *Nuclear Reactor Theory*. Robert E. Krieger Publishing Co. (1979).
35. Badhwar, G. *Radiation measurements in low earth orbit: U.S. and Russian results*. Health Phys. **79**, 507–514 (2000).
36. Bubble Technology Industries Inc. ***Report to the Canadian Space Agency***. Matroshka-R Project Final Report. Bubble Technology Industries (2008).
37. Bubble Technology Industries Inc. ***Report to the Canadian Space Agency***. Matroshka-R Experiment Phase 2. Bubble Technology Industries (2009).
38. Machrafi, R. *et al. Neutron dose study with bubble detectors aboard the international space station as part of the Matroshka-R experiment*. Radiat. Prot. Dosim. **133**(4), 200–207 (2009).
39. Lewis, B. J., Kosierb, R., Cousins, T., Hudson, D. F. and Guery, G. *Measurement of neutron radiation exposure of commercial airline pilots using bubble detectors*. Nucl. Technol. **106**, 373–383 (1994).
40. Vanderbilt University School of Engineering. CREME-MC. https://creme-mc.isde.vanderbilt.edu/CREME-MC (1996) (accessed 2010).
41. Koshiishi, H. *Evaluation of the neutron radiation environment inside the International Space Station based on Bonner Ball neutron detector experiment*. Radiat. Meas. **42**, 1510–1520 (2007).
42. Badhwar, G., Keith, J. and Cleghorn, T. *Neutron measurements onboard the space shuttle*. Radiat. Meas. **33**, 325–241 (2001).
43. D'Errico, F. *Radiation dosimetry and spectrometry with superheated emulsions*. Nucl. Instrum. Methods Phys. Res. B **184**, 229–254 (2001).
44. Bartlett, D. *The use of passive personal neutron dosemeters to determine the neutron component of cosmic radiation fields in spacecraft*. In: Proceedings of the 8th Workshop on Radiation Monitoring for the International Space Station, LBNL, Berkeley, CA, USA, 3–5 September (2003).
45. Simpson, J. A. *Introduction to the galactic cosmic radiation*. NATO ASI Ser. C: Math Phys. Sci. **107**, 1–24 (1983).
46. Sato, T., Niita, K., Iwase, H., Nakashima, H., Yamaguchi, Y. and Sihver, L. *Applicability of particle and heavy ion transport code PHITS to the shielding design of spacecrafts*. Radiat. Meas., **41**, 1142–1146 (2006).

APPENDIX

Response matrix for the SBDS

Response matrices from 0 to 50 MeV and 0–300 MeV (i.e. the latter derived from the high-energy iThemba data), based on the response data presented in Figure 17, is given below for spectral analysis with the SBDS.

Histogram interval (bubble/n cm^{-2})							
		j=1 (0.06–0.25)	j=2 (0.25–0.6)	j=3 (0.6–2.0)	j=4 (2.0–3.5)	j=5 (3.5–15)	j=6 (15–50) MeV
BDS-10	i=1	1.65E−05	4.00E−05	4.08E−05	4.08E−05	4.08E−05	4.08E−05
BDS-100	i=2	0	3.00E−05	3.50E−05	4.00E−05	4.20E−05	4.20E−05
BDS-600	i=3	0	0	2.00E−05	3.50E−05	4.20E−05	4.20E−05
BDS-1000	i=4	0	0	0	4.00E−05	6.00E−05	1.20E−04
BDS-2500	i=5	0	0	0	0	4.00E−05	1.10E−04
BDS-10000	i=6	0	0	0	0	0	1.00E−04
		j=l (0.06–0.25)	j=2 (0.25–0.6)	j=3 (0.6–2.0)	j=4 (2.0–3.5)	j=5 (3.5–15)	j=6 (15–300) MeV
BDS-10	i=1	1.65E−05	4.08E−05	4.08E−05	4.08E−05	4.08E−05	2.04E−05
BDS-100	i=2	0	3.00E−05	3.50E−05	4.00E−05	4.20E−05	2.10E−05
BDS-600	i=3	0	0	2.00E−05	3.50E−05	4.20E−05	2.10E−05
BDS-1000	i=4	0	0	0	4.00E−05	6.00E−05	6.00E−05
BDS-2500	i=5	0	0	0	0	4.00E−05	5.50E−05
BDS-10000	i=6	0	0	0	0	0	5.00E−05

These matrices are for a detector with a sensitivity of 0.1 bubble μSv^{-1}.